

**Original citation:**

Dinda, Soumitra Kumar, Basiruddin Sk, Md., Roy, Gour Gopal and Srirangam, Prakash. (2016) Microstructure and mechanical properties of electron beam welded dissimilar steel to Fe-Al alloy joints. Materials Science and Engineering: A . doi: 10.1016/j.msea.2016.09.050

**Permanent WRAP URL:**

<http://wrap.warwick.ac.uk/81655>

**Copyright and reuse:**

The Warwick Research Archive Portal (WRAP) makes this work by researchers of the University of Warwick available open access under the following conditions. Copyright © and all moral rights to the version of the paper presented here belong to the individual author(s) and/or other copyright owners. To the extent reasonable and practicable the material made available in WRAP has been checked for eligibility before being made available.

Copies of full items can be used for personal research or study, educational, or not-for-profit purposes without prior permission or charge. Provided that the authors, title and full bibliographic details are credited, a hyperlink and/or URL is given for the original metadata page and the content is not changed in any way.

**Publisher's statement:**

© 2016, Elsevier. Licensed under the Creative Commons Attribution-NonCommercial-NoDerivatives 4.0 International <http://creativecommons.org/licenses/by-nc-nd/4.0/>

**A note on versions:**

The version presented here may differ from the published version or, version of record, if you wish to cite this item you are advised to consult the publisher's version. Please see the 'permanent WRAP url' above for details on accessing the published version and note that access may require a subscription.

For more information, please contact the WRAP Team at: [wrap@warwick.ac.uk](mailto:wrap@warwick.ac.uk)

# Microstructure and mechanical properties of electron beam welded dissimilar steel to Fe-Al alloy joints

Soumitra Kumar Dinda<sup>a</sup>, Md. Basiruddin Sk<sup>a</sup>, Gour Gopal Roy<sup>a</sup>, Prakash Srirangam<sup>b\*</sup>

<sup>a</sup>Department of Metallurgical and Materials Engineering, Indian Institute of Technology, Kharagpur, India.

<sup>b</sup>Warwick Manufacturing Group (WMG), University of Warwick, Coventry, CV4 7AL, UK

\*Corresponding author: p.srirangam@warwick.ac.uk

## Abstract

Electron beam welding (EBW) technique was used to perform dissimilar joining of plain carbon steel to Fe-7%Al alloy under three different weld conditions such as with beam oscillation, without beam oscillation and at higher welding speed. The effect of weld parameters on the microstructure and mechanical properties of dissimilar joints was studied using optical microscopy, SEM, EBSD, hardness, tensile and erichsen cup tests. Microstructure results show that the application of beam oscillation resulted in uniform and homogeneous microstructure compared to without beam oscillations and higher welding speed. Further, it was observed that weld microstructure changes from equiaxed to columnar grains depending on the weld speed. High weld speed results in columnar grain structure in the weld joint. Erichsen cup test results show that the application of beam oscillation results in excellent formability as compared to high weld speed. Tensile test results show no significant difference in strength properties in all three weld conditions, but the ductility was found to be highest for joints obtained with the application of weld beam oscillation as compared to without beam oscillation and high weld speed. This study shows that the application of beam oscillations plays an important role in improving the weld quality and performance of EBW dissimilar steel to Fe-Al joints.

*Keywords: Electron beam welding, steel, Fe-Al alloy, microstructure, EBSD, mechanical properties, erichsen cup test, fractography.*

## 1. Introduction

The demand for the development of light weight materials has been increasing in automotive and aerospace industries to meet the challenges of fuel saving and greenhouse gas emissions. Hence, the transportation industry is in search of alternatives to meet these challenges and light weighting is the promising strategy in the field of automotive, nuclear, thermal power, chemical and petrochemical industries to enhance fuel efficiency and to reduce greenhouse gas emissions [1, 2, 3]. It is known that a reduction of 10% of total weight of the vehicle improves the fuel efficiency of passenger cars by 6-8% [4]. One method of reducing the weight of steel alloys is to add higher amounts of aluminium to steel. Addition of 7-8% aluminium reduces the density of steel by about 17% [5]. However, forming and welding of low density steels to other car body parts made of different alloy materials especially with steel parts is challenging due to the different physical, mechanical and metallurgical properties of dissimilar metals [6]. Arc welding processes which operates at very high heat input in comparison to EBW, favours the formation of different brittle Fe-Al intermetallics at the weld interface which deteriorates mechanical properties of weld dissimilar joints [7]. EBW is one of the best fusion welding processes which provides good mechanical and metallurgical properties in comparison to other welding processes such as friction stir welding, explosive welding, ultrasonic welding, arc welding, laser beam welding etc. [8, 9]. EBW has advantages such as high power density, low heat input, high penetration, low distortion, high depth to width ratio, narrow HAZ, less contamination from environments, and minimum amount of defects [10]. Due to low heat input, very high power density and

zero environmental contamination in EBW, the chances of defect formation is less in EBW dissimilar joints [11].

Optimisation of weld parameters is very important in welding process to achieve a sound weld quality with uniform microstructure and excellent mechanical properties of dissimilar weld joints. Metallurgical and mechanical property characterization of dissimilar welded joints is therefore essential to understand the influence of weld parameters on structure property relationships of joints. Suresh et al. studied EB-welding of thick Ti-6Al-4V alloy joints and found that the weld quality was improved with double sided welding as compared to single sided welding [12]. Babu et al. studied the effect of beam oscillations on the weld microstructure and mechanical properties of Ti-6Al-4V alloy system. They observed that the application of beam oscillations resulted in lower hardness and higher ductility in the weld region compared to without beam oscillation condition [13]. Sierra et al. studied the effect of weld parameters on mechanical properties of laser welded dissimilar joints of low carbon steel to aluminium alloy [14]. Bandhyopadhyay et al. studied the formability of laser welded high strength steel sheet joints by erichsen cupping test and validated the results with finite element modelling [15]. Kar et al. studied the effect of beam oscillation on the mechanical properties of EB-welded Cu-SS joint and reported that toughness of the joint increases significantly due to the application of weld beam oscillations [16]. Tomashchuk et al. studied the effect of weld parameters on the microstructures and mechanical properties of EB-welded titanium alloys to AISI 316L austenitic SS [17]. However, from literature review and past research studies, it was clear that the methods to improve microstructures and mechanical properties of EBW welded steel to Fe-Al alloy dissimilar joints has not been thoroughly studied in the past. In the present study, we aimed at understanding the effect of weld parameters on microstructure and mechanical properties of dissimilar steel to Fe-7% Al alloy

joints by EBW. Microstructural and mechanical properties characterisations were performed using optical microscopy, SEM, EBSD, hardness, tensile testing, and erichsen cup tests.

## 2. Experimental

### 2.1 Materials:

Plain carbon steel and Fe-Al alloys were used as base materials for EBW of dissimilar joining. Fe-Al alloy plates were supplied by Tata Steel R&D Corporation, Swindon, UK and steels were commercially purchased from N. Maity & Co., Kharagpur, India. Chemical analysis of base materials used in joining were analysed by X-ray spectroscopy analysis. Table 1 represents the chemical composition of base materials used in this study.

Table 1. Chemical composition of base materials in weight %.

Base Material	C	Al	Mn	Si	P	S	Nb	Ti	Fe
Fe-Al alloy	0.0044	6.94	0.20	-	-	-	0.01	0.01	Bal
Plain C-Steel	0.3	0.08	0.92	0.23	0.02	0.02	-	-	Bal

### 2.2 Preparation:

In order to perform welding, base materials were cut into 100 mm (L) x100 mm (W) dimensions having 1mm thickness of both side materials using diamond wheel cutter with water cooling system, mechanically polished using 320 grit emery papers and subsequently cleaned with acetone. Fig. 1 shows the schematic of EBW process with the application of beam oscillation. Beam oscillation was applied to modify the weld quality. Beam oscillation employs electromagnetic fields to alter the direction of electron beam as shown in Fig. 1b. Electron beam oscillation is an effective method to improve weld fusion and prevents molten

pool from collapsing and thereby reduces the root spiking of the welds [18]. The wave functions of beam oscillations were circle, triangle, and rectangle as shown in Fig. 1c.

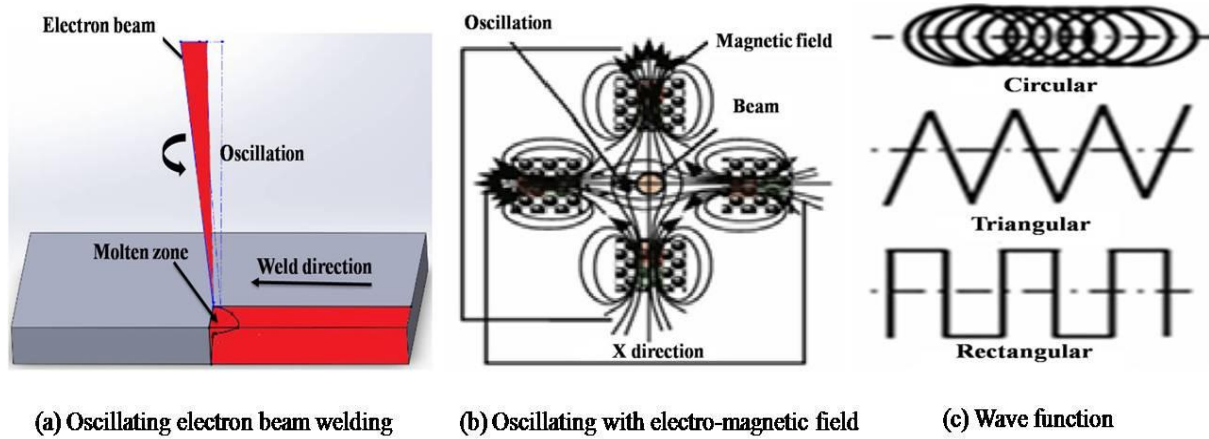


Fig. 1. Schematic of electron beam welding with beam oscillation [18].

### 2.3 Welding Procedure:

To accomplish the EB-Welding of steel to Fe-Al alloy dissimilar joints, bead-on plate welds were performed on three samples using EBW machine at Indian Institute of Technology, Kharagpur, India (developed by Bhabha Atomic Research Centre (BARC), Mumbai, India). Table 2 presents the list of various operating parameters used in EBW process.

Table 2. Parameters of EBW with full penetration of 1mm depth same for all three conditions.

Sample Condition	Beam voltage	Beam current	Welding speed	Oscillation		
	kV	(mA)	(mm/min)	Shape	Frequency (Hz)	Radius (mm)
With beam oscillation	60	17	1000	Circle	600	0.5
Without beam oscillation	60	17	1000			
Higher welding speed	60	19.6	1500			

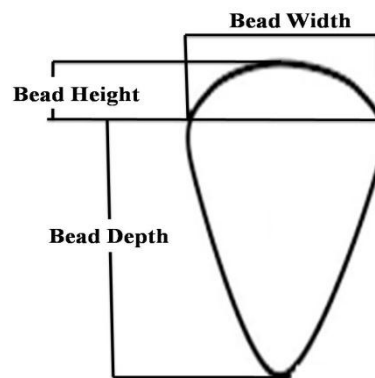


Fig. 2. Schematic of weld pool geometry.

Fig. 2. shows the schematic of weld pool geometry showing the bead depth, bead width and bead height. Table 3. presents the different weld processing variables used in EBW of dissimilar steel to Fe-7% Al alloy.

Table 3. Electron Beam Welding process variables.

Gun chamber vacuum(mbar)	$10^{-6}$	Gun-specimen distance (mm)	465
Welding chamber vacuum (mbar)	$10^{-5}$	Welding pass	1
Both material dimensions (mm <sup>3</sup> )	100 x 100 x 1		

#### 2.4 Microscopy characterisation:

Microstructural characterisation studies were performed on welded samples using optical microscopy and SEM. Samples for microscopy were mechanically polished and etched using two different types of etchants. Steel side of the joint was etched by 2% Nital (2ml HNO<sub>3</sub>+98ml C<sub>2</sub>H<sub>5</sub>OH) while Fe-Al side of the joint was etched by an etchant of 33% CH<sub>3</sub>COOH + 33% HNO<sub>3</sub> + 33% H<sub>2</sub>O+ 1% HF [19]. First Fe-Al alloy base metal and weld bead etched by above etchant and then it covered by nail polish. After that steel side etched by 2% Nital. Microstructures were taken after removing the nail polish using ethyl alcohol (C<sub>2</sub>H<sub>5</sub>OH). Grain size measurements were carried out using grain intercept method. SEM & EBSD analysis was carried out using HKL Channel 5 system (fitted in Zeiss® EVO 60 SEM) from Oxford Instruments, UK, operated at a step size of 2.5 µm.

#### 2.5 Hardness measurements:

Microhardness measurements were performed using Wilson hardness testing machine. Hardness measurements were taken along the transverse direction of weld bead, heat affected zone (HAZ) and fusion zone (FZ) using a diamond pyramid indenter under a load of 100g with a dwell time of 20sec.

#### 2.6 Tensile testing:

Tensile tests were performed out using Instron tensile testing machine with 5kN maximum load capacity fitted with a digital extensometer. A strain rate of 0.06mm/min was used in

tensile testes for all three weld samples as well as for base metals. For each weld condition, tests were repeated three times to report the average values with standard deviation. Fig. 3 represents the schematic of ASTM E-8 sub-size standard tensile specimen geometry.

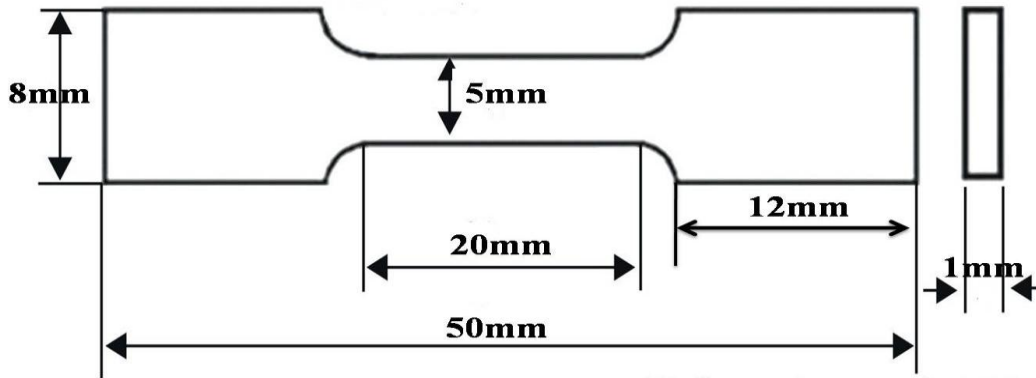


Fig. 3. Schematic of tensile specimen geometry.

### 2.7: Erichsen cup testing:

Erichsen cup tests were carried out at room temperature to evaluate out-of-plane stretch forming behaviour dissimilar welded samples. The cup heights and thickness distributions were measured to study the effect of weld parameter on room temperature formability. Samples of 70 mm x 70 mm were cut from all three weld conditions. Erichsen cup tests were performed using a 20mm diameter hemispherical punch in the Erichsen testing machine made by Akash Industries, Maharashtra, India. Grease was applied as a lubricant between the sample and punch to induce biaxial strain state during stretch forming. Tests were carried out by placing the weld seam exactly in the middle of die and the weld root pointing towards the punch. The upper die was pressed over the blanks to keep the blank in proper position and to restrict the flow of material from the die flange during testing. All tests specimens were stretched till the initiation of crack and the cup height was measured using height gauge with a least count of 0.01 mm. Thickness distributions were measured after cutting the cup perpendicular to the crack plane. Cup cutting was performed using EDM wire cutting

machine. The cup heights and thickness distributions were measured to study the effect of weld parameter on room temperature formability of dissimilar joints.

### 3. Results and discussion

#### 3.1 Micro structural analysis

##### 3.1.1 Base metal

Fig. 4 shows the optical microscopy images representing the microstructure of base materials prior to welding. As shown in Fig. 4a, microstructure of Fe-Al alloy base metal exhibits Fe-Al ( $\alpha$ ) single phase microstructure with grains oriented in the rolling direction of the plate. Similar observations were made by Khaple et al. [20] in their microstructural studies of Fe-Al alloy. No intermetallic compounds were observed in Fe-7%Al alloys. As shown in Fig. 4b, the microstructure of plain carbon steel was composed of ferrite and pearlite.

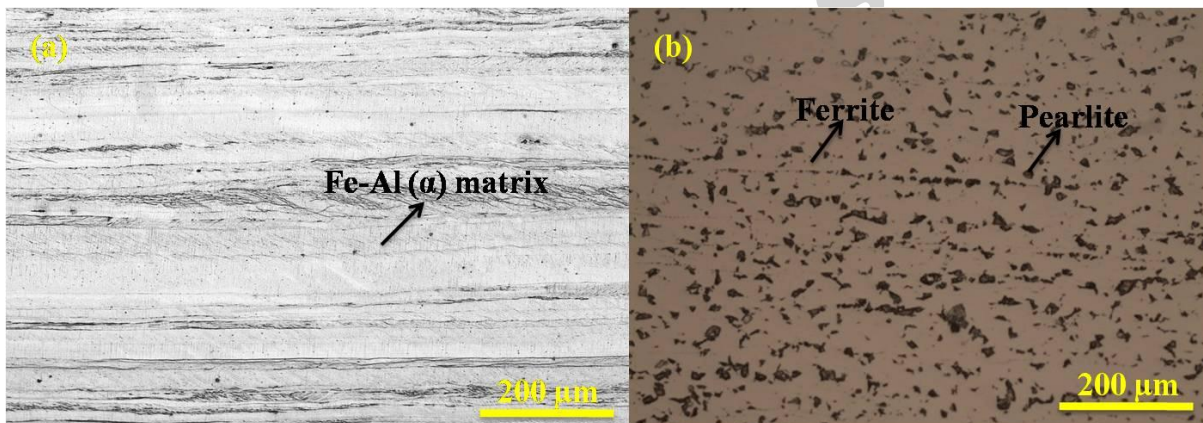


Fig. 4. Microstructure of base materials: (a) Fe-7%Al alloy (b) plain carbon steel

##### 3.1.2 Fusion zone

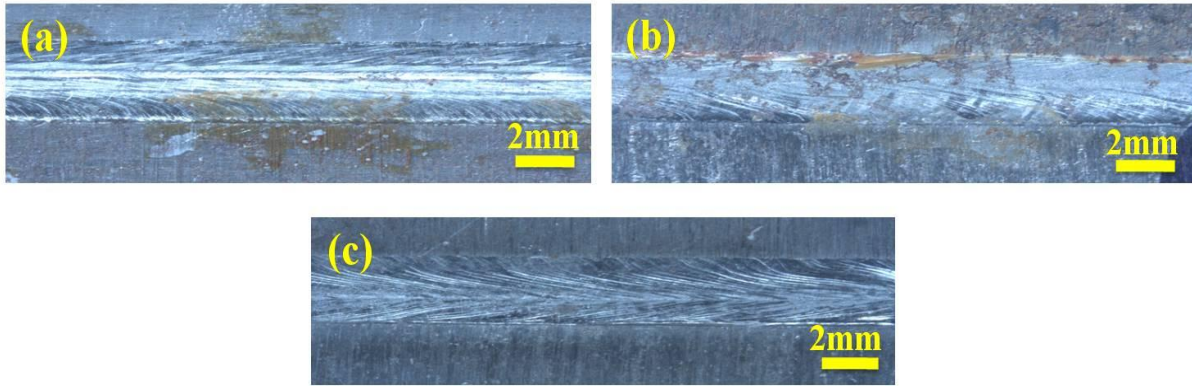


Fig. 5. Surface appearance of weld bead under different weld conditions (a) with beam oscillation, (b) without beam oscillation, (c) higher welding speed.

Fig. 5 shows the surface appearance of weld bead under three different weld conditions. As shown in Fig. 5a, the application of beam oscillation resulted in smoother weld bead as compared to without beam oscillation and higher welding speed condition as shown in Fig. 5b & 5c respectively.

Table 4 Measured weld bead and calculated heat input comparison for all three conditions

Sample Condition	Measured weld bead	Calculated Heat Input
	mm	kJ/mm
With beam oscillation	2.69	0.0612
Without beam oscillation	2.23	0.0612
Higher welding speed	2.15	0.0473

Table 4 presents the variation of weld bead for three different EBW dissimilar joints. As shown in Table 4, for the same amount of heat input, application of beam oscillation resulted in increase in weld bead as compared to without beam oscillations. The weld bead was found to be 2.69 mm in the case of with beam oscillations, while it was found to be 2.23 mm, in the

case of without beam oscillations. Increase in weld speed narrowed the weld bead (2.15 mm) as compared to lower weld speed (2.23 mm). Also, the striations were found to be higher with increase in weld speed. Similar observation were made by Kar et al. [21] that increasing welding speed results in decreasing the weld bead in Cu-SS dissimilar electron beam welded joints.

### 3.1.3 Macrostructure & microstructure of welded joints

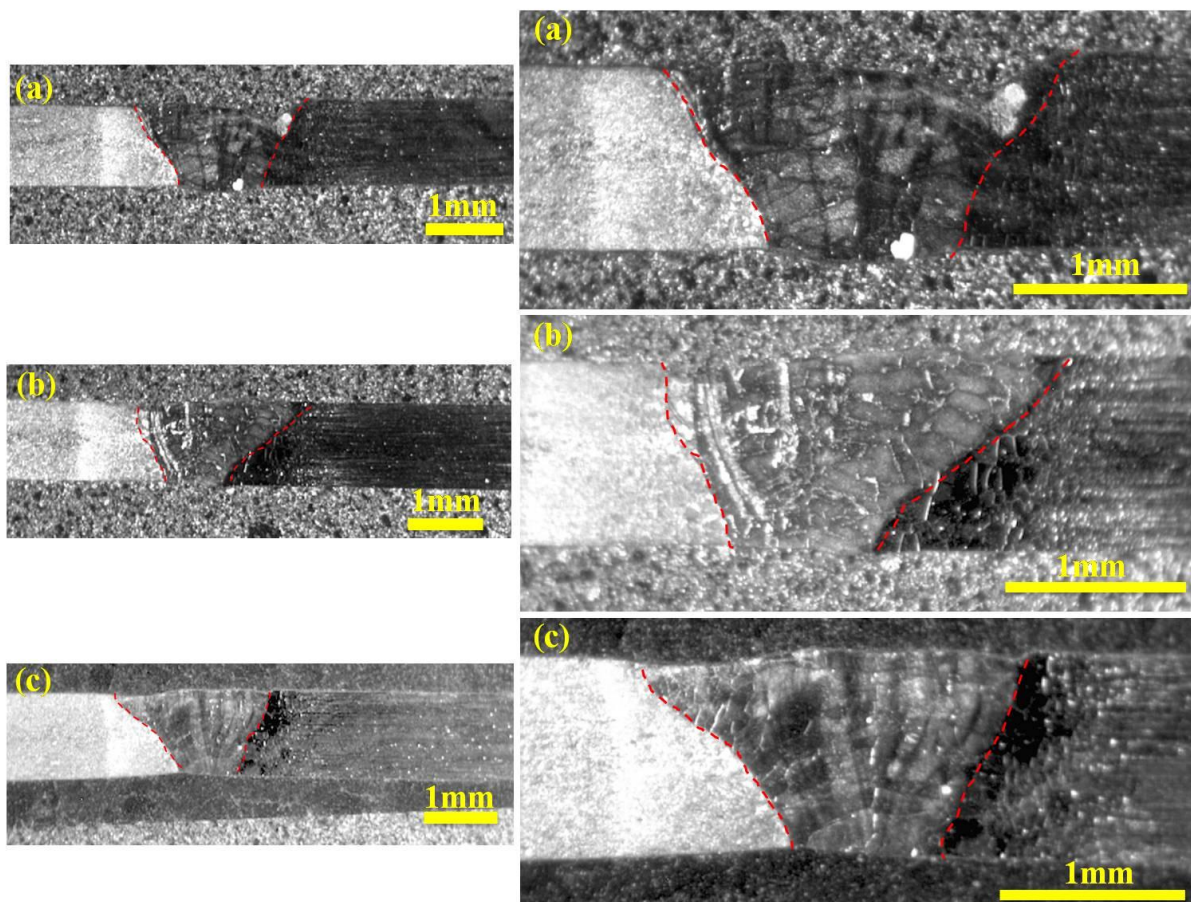


Fig. 6. Optical macrostructure at lower (left) & higher (right) magnification with fusion boundary (red dotted line) of weld bead after etching (a) with beam oscillation, (b) without beam oscillation, (c) higher welding speed.

Fig. 6 represents the macrostructures of etched welded samples for three different conditions showing a clear boundary between the fusion zone and base metals at lower and higher magnifications. Fig. 7a to Fig. 7c represents the optical microstructure of dissimilar joints for three different weld conditions. As shown in figures, there exists a sharp transition between base metal and fusion zones having very little HAZ compare to other conventional welding processes. Columnar grain structure was formed in the fusion boundary and extended to the centreline of the weld joint, while the grain size was unaffected in base metals.

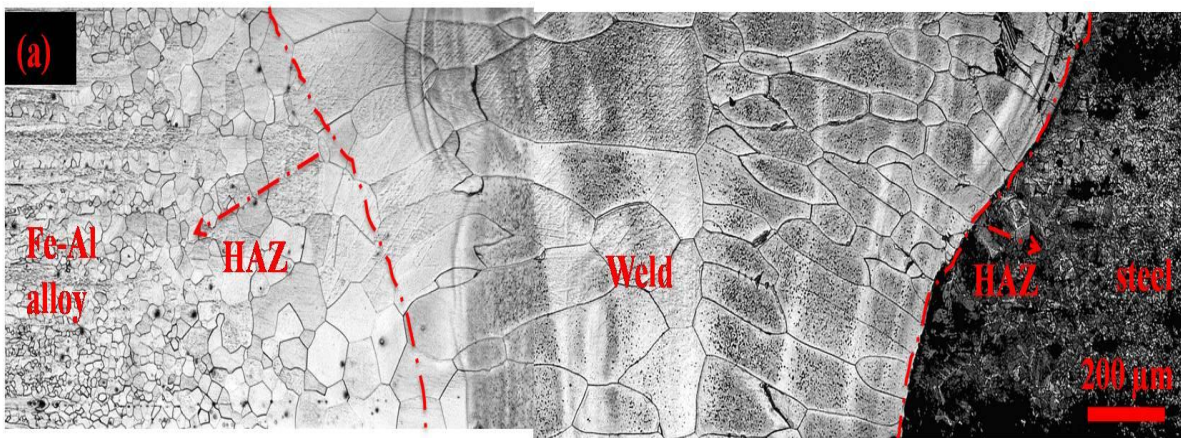


Fig. 7.(a) Optical microstructure of different regions of dissimilar joint with the application of beam oscillation. (b) Optical microstructure of different regions of dissimilar joints under without beam oscillation condition. (c) Optical microstructure of different regions of dissimilar joint at higher welding speed condition.

In the weld interface region of steel side of base metal, pearlite phase could be seen with less ferrite phase formed on pearlite grain boundaries, while in Fe-Al alloy side, Fe-Al ( $\alpha$ ) single phase was observed. Microstructure in weld zone and base metals to weld zone shows the formation of larger grains due to the application of beam oscillation in the welding process.

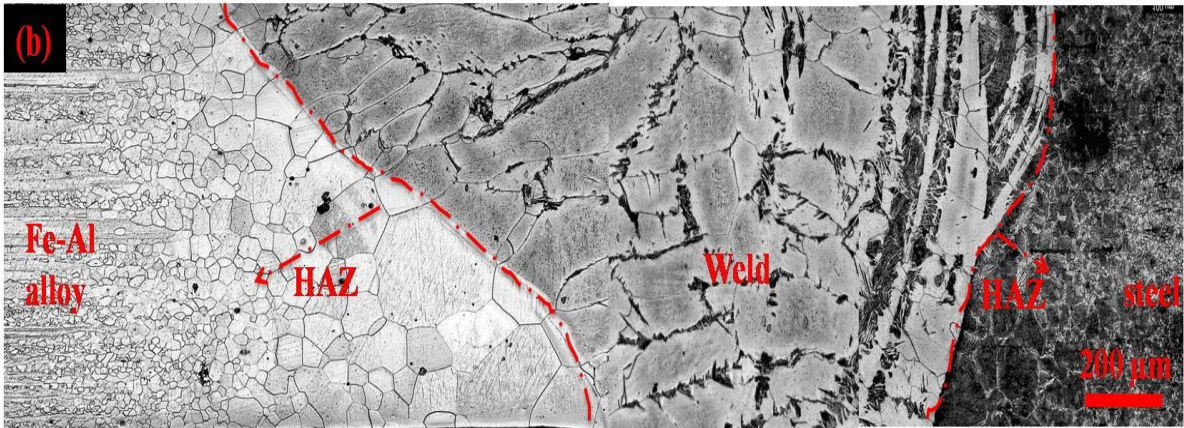
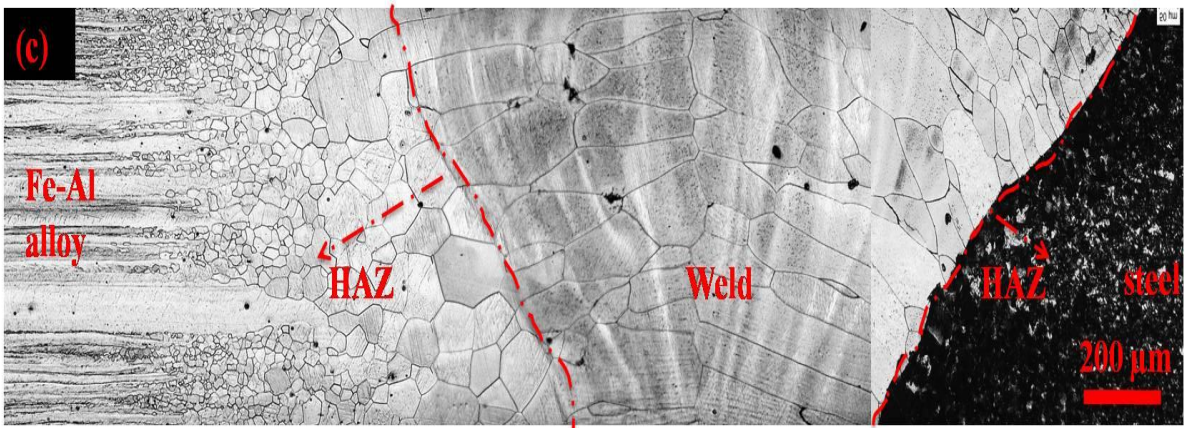


Fig.7b shows optical microscopy images of different weld regions for EBW dissimilar joint without the use of beam oscillations. Microstructure shows coarse and more equiaxed grains in the weld joint. Due to more time during welding at without beam oscillation condition, elemental distribution of carbon into the weld was prominent but not uniform throughout the welded region. Carbon depletion took place at grain boundaries in weld region which was not observed in Fe-Al side weld zone due to very low carbon content in Fe-Al alloy.



Higher welding speed results in fine columnar grain structure throughout the weld zone as shown in Fig. 7c. Higher the weld speed under without beam oscillation results

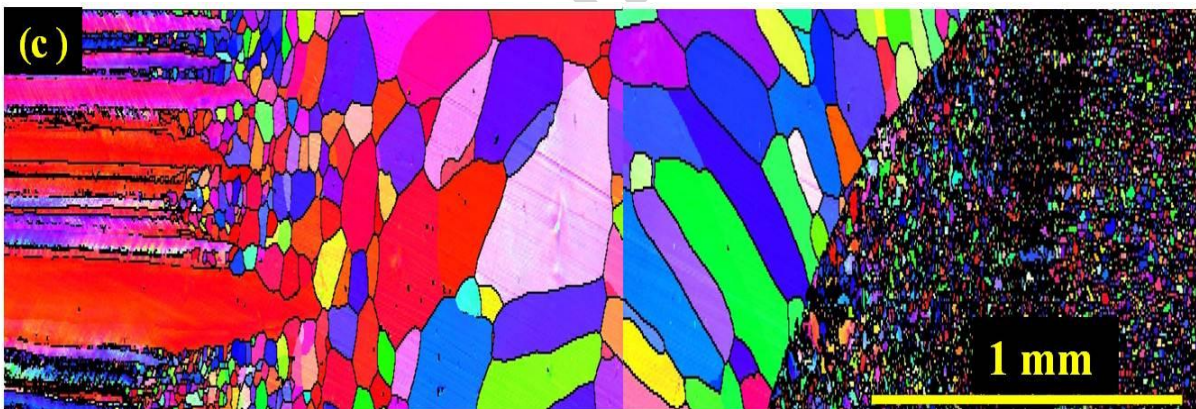
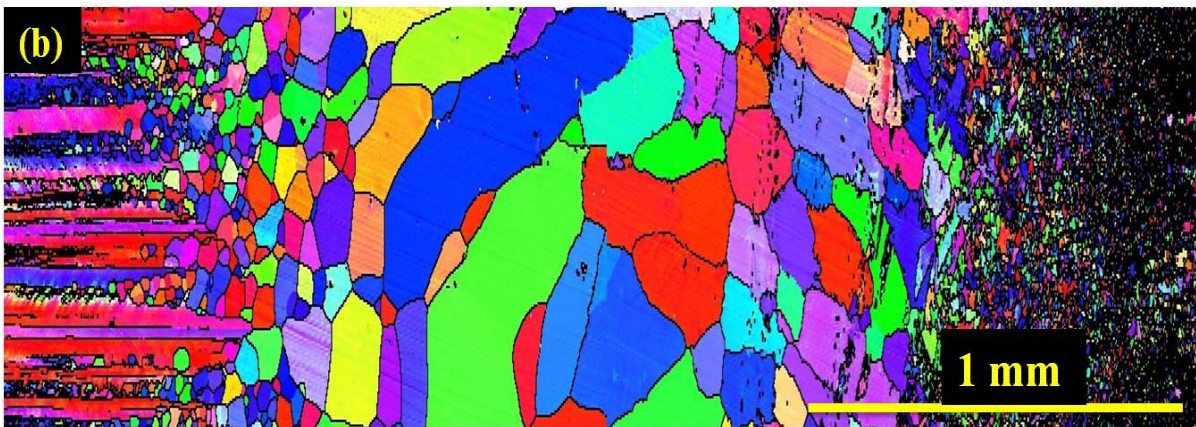
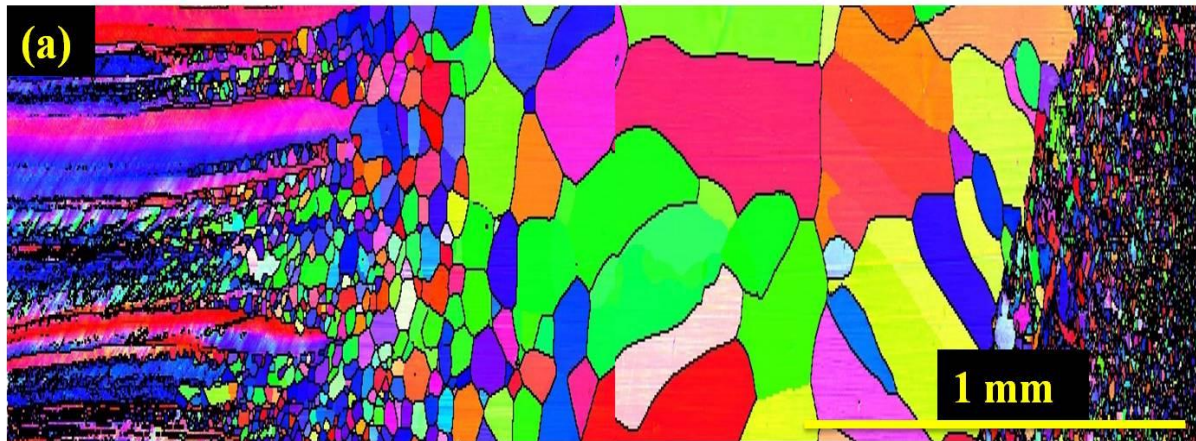
inhomogeneous mixing of temperature and alloying elements which results in non-uniform microstructure in the joint. Higher the weld speed, lesser the time for coarsening of grains which results in fine grain structure in the weld joints. It was clear from Fig. 7a to Fig. 7c that the application of beam oscillations results in uniform and homogeneous microstructure compared to other two weld conditions.

Table 5 Average grain size in different weld regions for three weld conditions (in  $\mu\text{m}$ )

Sample condition	HAZ(Fe-Al alloy)	Weld portion	HAZ (Plain C-Steel)
With beam oscillation	63	207	33
Without beam oscillation	51	171	30
Higher welding speed	43	128	29

The average grain size was found to be highest with beam oscillation condition, while it was found to be lowest in case of higher weld speed condition. As reported by kar et al. welding with the application of beam oscillation could be considered as of solidification of several tiny weld pools with significant overlapping between those pools [16]. Such overlapping introduces an effect of preheating of each pool which reduces the cooling rate leading to coarser grain size formation in the joint. Due to better mixing at with beam oscillation condition, the chances of formation of columnar grains would be less, and highest in case of higher welding speed condition. Similar observations were made by Fu et al. that the application of beam oscillation resulted coarser more homogeneous microstructure in weld

joint[18].



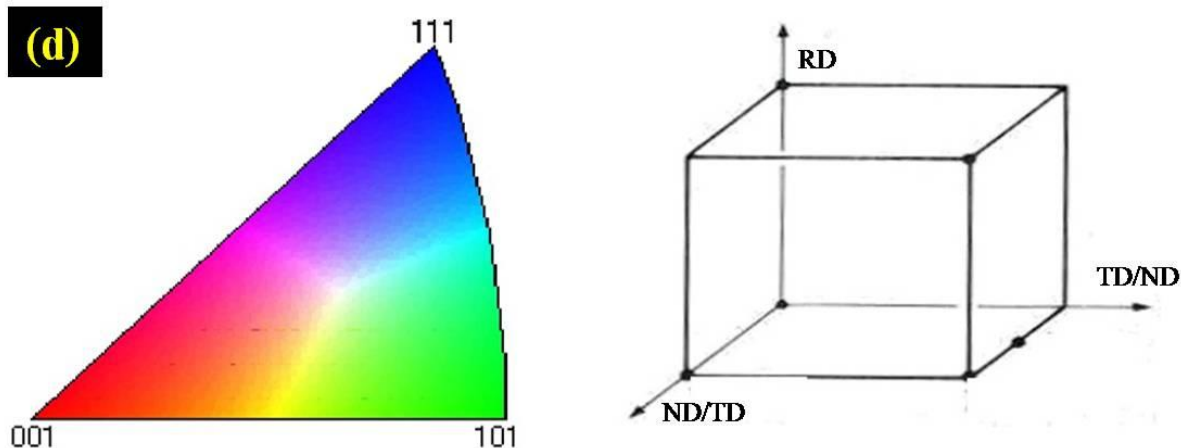


Fig. 8. EBSD maps of weld joints in different conditions (a) with beam oscillation (b) without beam oscillation (c) higher welding speed; (d) Unit triangle of the inverse pole figure showing the crystal alignment with respect to the rolling direction (RD) of welded joints.

Fig. 8 represents the EBSD analysis of all three dissimilar welded samples. As shown in Fig. 8, color maps indicate the crystallographic orientation of grains in all welded samples. The colors in the stereographic triangle indicate that the crystallographic orientation was parallel to rolling direction (RD). EBSD results represent the grain size variation across the weld zone from base metal of Fe-Al alloy to the base metal of steel side. From inverse pole figure map as shown in the Fig. 8, a clear boundary between weld zones to base metal at steel side had been observed which indicate a sharp change in grain size but a gradual decrease in grain size from weld to Fe-Al alloy base metal side. From this pole figure map, we can say that an inhomogeneous mixing had occurred in weld zone to steel side as compared to Fe-Al alloy to weld side. Fig. 8a shows the EBSD analysis of dissimilar joints at with beam oscillation condition. As shown in Fig. 8a, majority of grains were oriented in  $101 \parallel \text{ND}$  and  $001 \text{ (bcc)} \parallel \text{ND}$  (normal direction) from weld zone to steel side, which results in less deformation due to less number of slip systems. Fig. 8b represents the EBSD results of dissimilar joint without beam oscillation condition. As shown in Fig. 8b, majority of grains oriented in  $111 \text{ (fcc)} \parallel \text{ND}$  and  $101 \parallel \text{ND}$  which promotes easy movement of dislocations due to closed packed slip

systems. Fig. 8(c) shows EBSD results of dissimilar joint at higher welding speed condition. As shown in Fig. 8c, grains were oriented in  $111$  (fcc)  $\parallel$  ND and  $101 \parallel$  ND similar to without beam oscillation condition. Here, grains were elongated form which provides less deformation compared to without beam oscillation condition. In fusion zone, due to high power input, metals becomes molten in a very small area which results in epitaxial solidification with grains oriented perpendicular to weld direction. In HAZ, the elongated ferrite grains at Fe-Al alloy side get recrystallized resulting in the formation of finer grain structure in HAZ. The reason for recrystallization of ferrite grains in Fe-Al side HAZ is due to the presence of greater amount of internal stresses that were generated during processing of alloy sheet. Whereas, in HAZ at steel side, no such recrystallization was observed as low carbon steel sheet was hot deformed which reduces the formation of internal stresses by dynamic recrystallization, and hence no further recrystallization was observed during welding.

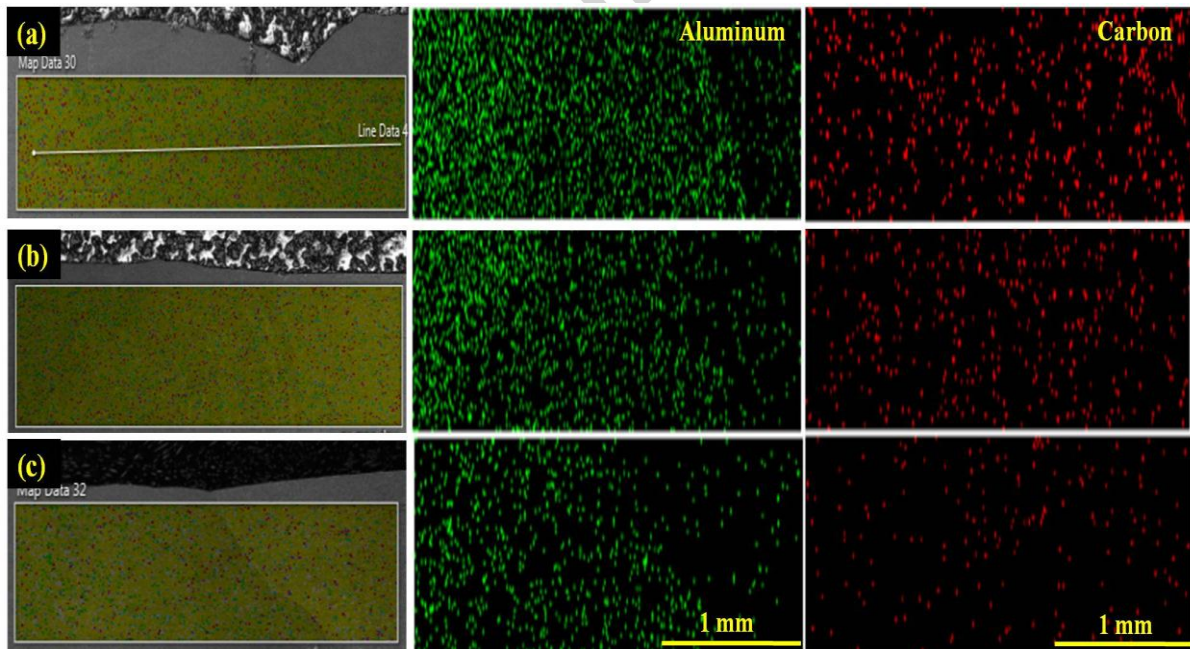


Fig. 9. SEM-EDS area map profile of Aluminium-K $\alpha$  and Carbon-K $\alpha$  of (a) with beam oscillation, (b) without beam oscillation and (c) higher welding speed.

The area mapping of major alloying elements i.e. aluminium and carbon obtained from the EDS analysis throughout the sample provides information about elemental distribution as shown in Fig. 9. Considering the elemental distribution of aluminium, the interface between base metal and weld zone was barely visible in case of with beam oscillations as shown in Fig. 9a. Area mapping shows that aluminium rich region exists near the Fe-Al alloy side of fusion zone with a negligible amount of carbon dispersed in both HAZ and weld region of Fe-Al side, while carbon rich regions exists at steel side of fusion zone compared to Fe-Al alloy side. As shown in fig. 9(a), it can be observed that the application of beam oscillation resulted in uniform dispersion of both aluminium and carbon were in the weld zone compared to other two conditions. Due to the slow cooling rates associated in case of without beam oscillation condition (Fig. 9b), alloying elements i.e. aluminium and carbon were diffused in weld region compared to with beam oscillation and higher welding speed conditions. But, better and uniform mixing of alloying elements was observed with the application of beam oscillations during welding due to churning action of molten pool associated with beam oscillations. As shown in Fig. 9c, higher the weld speed resulted in poor dispersion of aluminium and carbon due to short time for inter-diffusion of alloying elements in the weld region. Kar et al. used beam oscillations in EBW of Cu-SS joints for the improvement of microstructure and found that application of beam oscillation results in improving weld quality as compared to without beam oscillation condition [16]. Table 5 shows the average grain size measured from optical images in different weld regions for three weld conditions.

## **3.2 Mechanical property characterization**

### **3.2.1 Hardness measurements**

Fig. 10 represents the hardness of EBW dissimilar joints for three weld conditions. It was clear from Vickers hardness measurements that Fe-Al alloy base metal had high hardness and decreased towards weld zone.

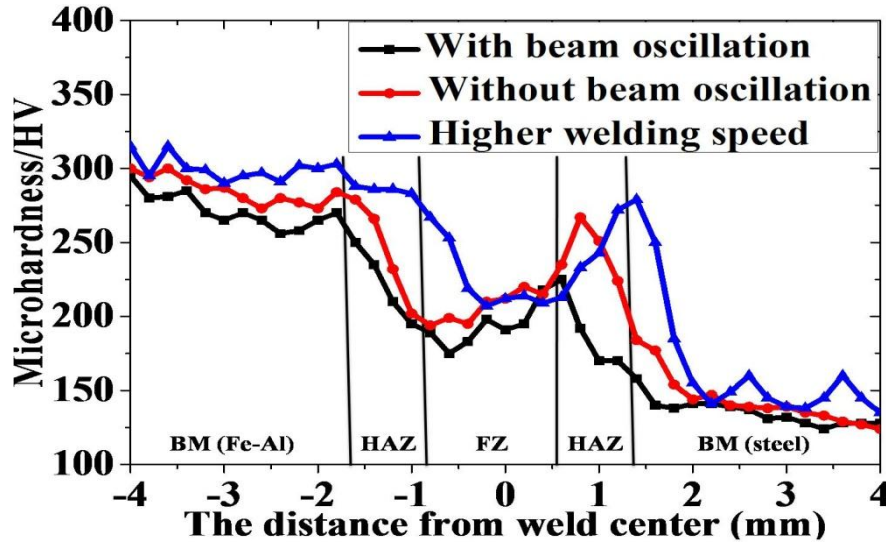


Fig. 10. Variation of micro hardness of EBW dissimilar joints for three different weld conditions.

As shown in Fig.10, the average hardness value of Fe-Al alloy base metal was 285 Vickers pyramid number (HV), whereas the hardness value of plain carbon steel was 140 HV. It is visible that the hardness value of base metals was not affected significantly due to change in weld condition. The hardness found to be decreasing while moving from Fe-Al to HAZ and this decrease was more significant with increasing weld speed. On the other side i.e. steel side, hardness found to be increasing from steel side to HAZ and this increase was more significant in case of higher weld speed. Hardness at weld zone was highest in case of higher welding speed (230 HV) compare to other two cases i.e. without beam oscillation (210 HV) and with beam oscillation (195 HV). Hardness value from Fe-Al alloy base side to HAZ region decreased due to coarse grains formation in the microstructure as shown in Fig 8. From weld to steel side, in the HAZ region, hardness value increased due to the decrease in grain size and more importantly due to carbon diffusion from steel side to HAZ region which contributed as grain boundary strengthening by increasing carbon equivalent which gave high

hardness value [22]. At higher welding speed, hardness values were observed which could be due to formation of fine grain structure with high weld speed. These observations were consistent with previous research studies where it was shown that increasing welding speed results in increase in hardness value of weld joints [23].

### 3.2.2 Tensile measurements

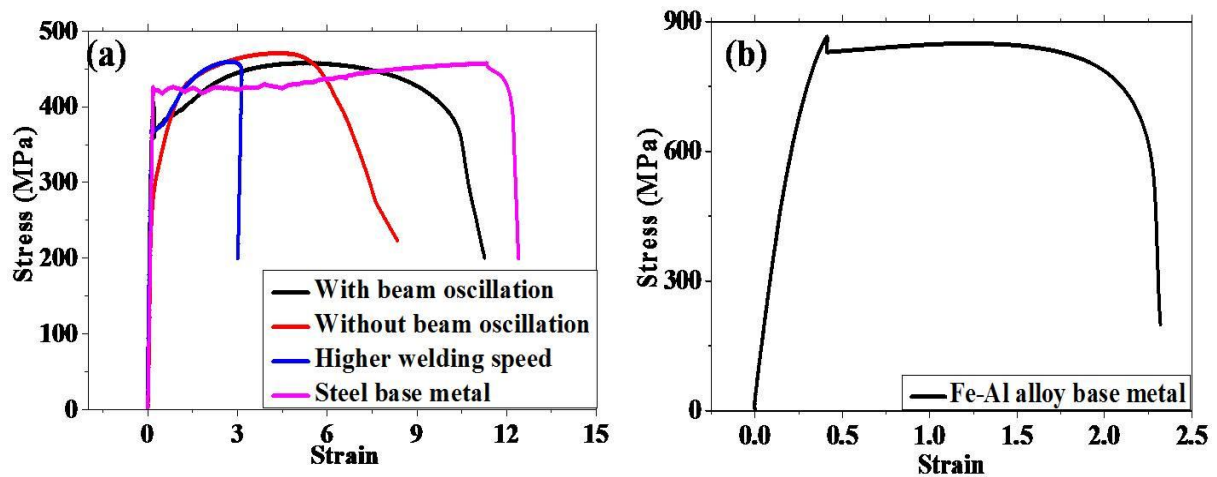


Fig. 11. Stress-strain diagram (a) for three weld conditions and steel base metal, (b) Fe-Al alloy base metal.

In order to understand the service performance of weld dissimilar joints, tensile tests were carried out at room temperature. Fig. 11 shows the stress vs strain diagrams of dissimilar joints for different weld conditions. For comparison, stress-strain diagram of Fe-7%Al was plotted as shown in Fig. 11b. Table 6 shows the measured values of YS, UTS, and percentage elongation of dissimilar weld joints for three weld conditions. It was clearly observed that even though all samples had almost similar YS and UTS values, but the percentage of elongation was found to be varying with weld condition. It was found that the application of beam oscillation resulted in higher percentage of elongation (12.9%) as compared to without beam oscillation (9.67%) and higher welding speed (2.87%) conditions. Higher percentage of

elongation under beam oscillation condition was due to uniform microstructure, compositional distribution that enhances tri-axiality of stress condition that suppresses cracking due to stress concentration. As shown in Fig. 11b, the YS (813 MPa) and UTS (865 MPa) of Fe-Al alloy base metal was quite high compared to all weld conditions.

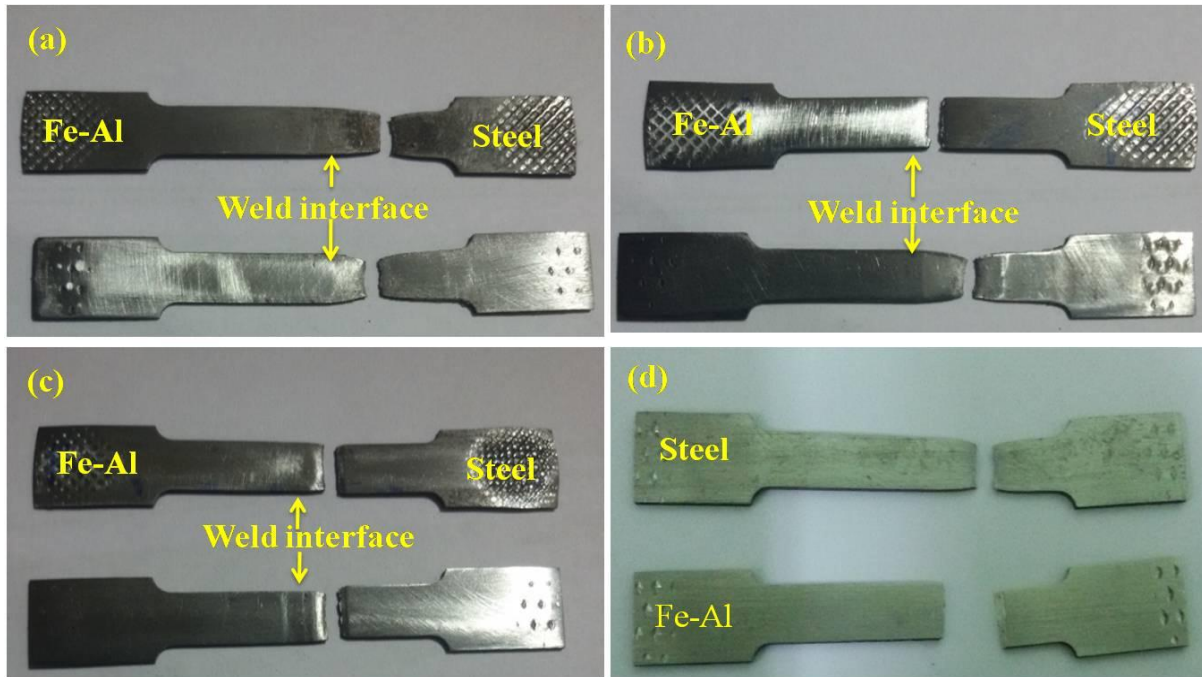


Fig. 12. Photograph of the fractured tensile tested specimens of three welded samples (a) with beam oscillation, (b) without beam oscillation (c) higher welding speed and (d) base metal of both sides.

Fig. 12 shows the fractured surfaces of tensile tested samples. It was observed that the fracture occurred close to steel base metal side during tensile testing for all three weld conditions.

Table 6 YS, UTS and Percentage elongation of dissimilar weld joints under different weld conditions.

Sample Description	YS (MPa) (± error)	UTS (MPa) (± error)	% elongation (± error)	Failure Location
With beam oscillation	370±3.6	471± 3	12.95±0.7	Steel side (away from weld)
Without beam oscillation	327 ±6.3	458 ±6.6	9.67 ±0.6	Steel side
Higher welding speed	378 ±7.6	460 ±8.2	2.87 ±0.9	Steel side (near to weld)
Steel plate	450 ±13	459 ±15	14.09 ± 0.4	In gauge
Fe-Al plate	813 ±11	865 ±12	2.47 ±0.6	In gauge

Fig. 13 represents the fractography images of tensile specimen of dissimilar joints under three different weld conditions as well as for base metals. Fig. 13a, b and c shows the fracture surfaces for with beam oscillation, without beam oscillation and high weld speed. From fractography images, it was clear that small and deeper dimples were distributed on fracture surface of sample with beam oscillation as compared to other two weld conditions. This represents that the fracture mode in case of beam oscillation was ductile in nature which was consistent with tensile test results where application of beam oscillation shown highest elongation compared to other two weld conditions. In case of without beam oscillation, (Fig. 13b) fracture surface shows a combination of ductile and brittle mode of fracture, where as a perfect brittle type of fracture mode was observed in case of higher welding speed as in Fig. 13c due to high hardness value. Further, it was observed that the fracture mode of steel base metal was perfectly ductile while Fe-Al alloy base metal exhibits a perfect brittle type fracture as shown in Fig. 13d and 13e respectively. Kar et al. [16] investigated the effect of beam oscillation on welded joints of Ti-6Al-4V alloy and found that the application of weld beam oscillation shows ductile type of fracture mode and these results were consistent with our fractography studies on dissimilar joints.

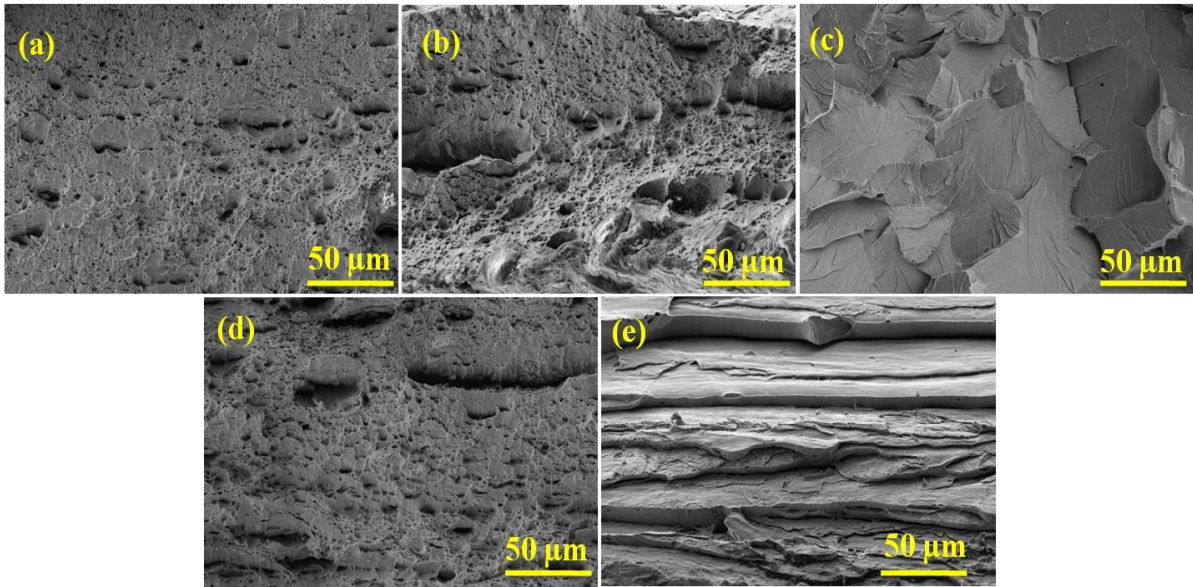


Fig. 13. Fractography images of dissimilar joints (a) with beam oscillation, (b) without beam oscillation, (c) higher welding speed, (d) steel base metal, (e) Fe-7%Al base metal.

### 3.2.3 Ericson cupping test

#### 3.2.3.1 Erichsen Cup Height

Fig. 14 represents the deformed specimens from erichsen cup tests of three different welded samples. It was evident that the failure occurred quite close to centre portion of welded materials which means a biaxial type of deformation during cup test. Necking was observed during deformation of all three samples, which led to eventual failure on further deformation. Among all three weld conditions, the erichsen cup height of the sample with beam oscillation has deformation height (5.67mm) compared to without beam oscillation (4.72mm) and higher welding speed (3.17mm) due to homogeneous and uniform microstructure that was observed in case of with beam oscillations.

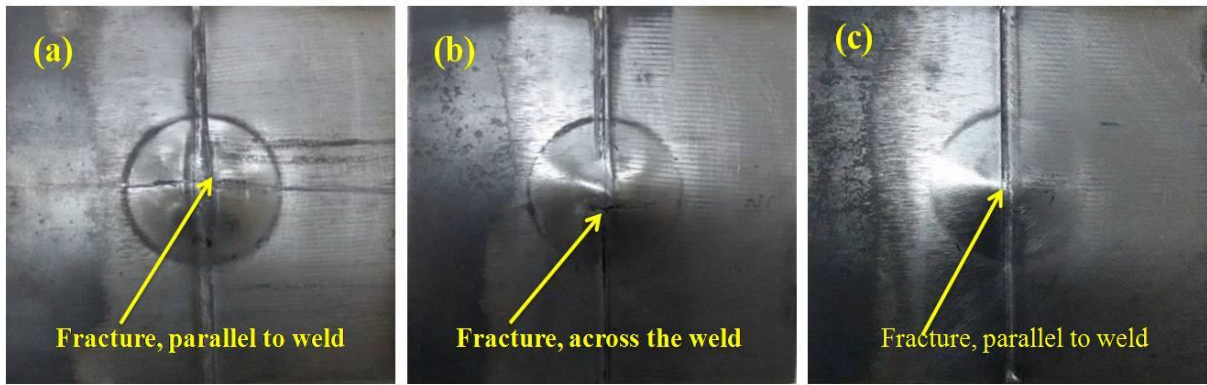


Fig. 14 Deformed cups from Erichsen cup tests showing failure location in (a) with beam oscillation, (b) without beam oscillation, (c) higher welding speed.

### 3.2.3.2 Thickness Distribution

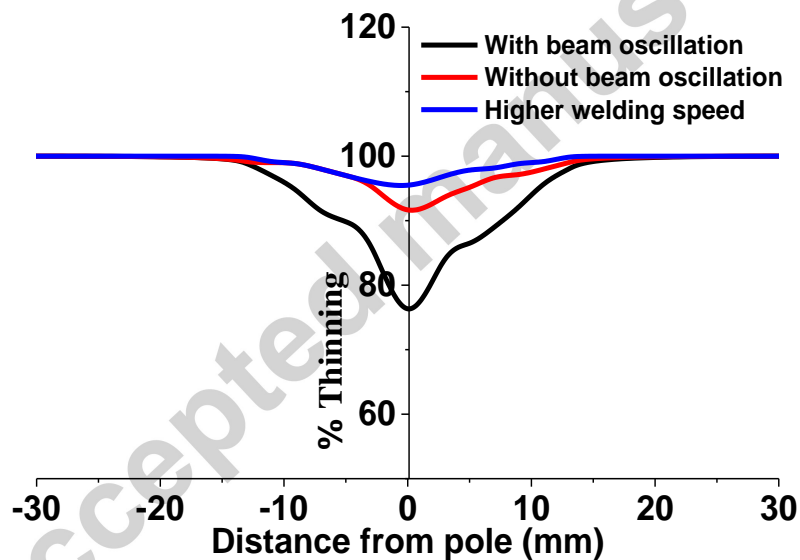


Fig. 15. Shows comparison of percentage (%) thinning in deformed cups of three different welded samples.

The thickness distributions from experimental cup section were measured and compared for all three welded conditions. The percentage of thinning with respect to original thickness in the deformed cups was calculated (measured thickness $\times$ 100/original sheet thickness) over the cup surface after measuring the thickness at several distances from the pole along a direction

perpendicular to crack propagation. An abrupt thinning took place at the cup corner where the sheet metal bent over the die profile radius in the erichsen cup tester. Then, the thickness gradually decreased over the dome leading to thinning and final fracture close to the pole. It was clear from Fig. 15 that among all three conditions, the sample with beam oscillation had shown highest percentage of thinning compared to other two weld conditions. Higher weld speed shown poor response to erichsen cup test with poor formability as compared to other two weld conditions as shown in Fig. 15. Higher the weld speed, finer the grain size and higher the hardness in weld joint which ultimately results in poor formability. Presence of different types of weld defects such as porosity could also adversely affect the mechanical properties of the weld joints. In our recent study on porosity formation in EBW dissimilar joints of the same materials showed that. Among all weld conditions, application of beam oscillation improved the weld quality with less porosity formation in the weld joint. This could be also the reason for showing good microstructure formation with excellent mechanical and deformation properties as observed in this study for weld condition with beam oscillations compared to without beam oscillation and weld speeds.

#### **4. Conclusions**

In this paper, dissimilar metals joining of Fe-7%Al alloy to plain carbon steel was performed by electron beam welding process under different weld conditions such as with beam oscillations, without beam oscillations and at higher welds speed. Following conclusions were drawn from the present study:

1. Microstructural characterisation shows that the application of beam oscillation results in uniform and homogeneous microstructure as compared to without beam oscillations. Increasing welding speed resulted in fine grain structure in the joint.

2. Microhardness results show that among all three weld conditions, the application of beam oscillations provide low hardness value compared to without beam oscillation and higher welding speed condition.
3. Though the YS and UTS of welded samples is unaffected in all three conditions, but the percentage of elongation was found to be high in case of with beam oscillation as compared to other two weld conditions. Also, fractography results show that the mode of fracture was ductile in case of with beam oscillations, while it was found to be brittle with high weld speeds.
4. Erichsen cup test results show that the application of beam oscillation resulted in good formability properties as compared to without beam oscillation and at higher weld speed.

### **Acknowledgements**

We thank Dr. Arunansu Haldar of Tata Steel, Rotherham, UK and Prof. S. Sridhar, WMG, University of Warwick for providing Fe-Al alloy samples and for their suggestion during preparation of the manuscript. We thank UKERI (UK-India collaborative project) and Prof. Richard Dashwood of WMG for their financial support in carrying out this research work.

### **References**

- [1] W. S. Miller, L. Zhuang, J. Bottema, A. J. Wittebrood, P. De Smet, A. Haszler, A. Vieregge, Recent development in aluminium alloys for the automotive industry, *Materials Science and Engineering: A*. 280 (2000) 37–49. doi:10.1016/S0921-5093(99)00653-X.

- [2] R. S. Coelho, A. Kostka, J. F. dos Santos, A. Kaysser-Pyzalla, Friction-stir dissimilar welding of aluminium alloy to high strength steels: Mechanical properties and their relation to microstructure, *Materials Science and Engineering A*. 556 (2012) 175–183. doi:10.1016/j.msea.2012.06.076.
- [3] T. Watanabe, H. Takayama, A. Yanagisawa, Joining of aluminum alloy to steel by friction stir welding, *Journal of Materials Processing Technology*. 178 (2006) 342–349. doi:10.1016/j.jmatprotec.2006.04.117.
- [4] W. J. Joost, Reducing vehicle weight and improving U.S. energy efficiency using integrated computational materials engineering, *Jom*. 64 (2012) 1032–1038. doi:10.1007/s11837-012-0424-z.
- [5] S. Chaudhary, S. Khaple, V. V. Satya Prasad, A. Sambasiva Rao, R. G. Baligidad, Effect of Titanium and Carbon on Microstructure and Mechanical Properties of Disordered Solid Solution Fe–7 wt% Al Alloy, *Transactions of the Indian Institute of Metals*. (2015) 13–16. doi:10.1007/s12666-015-0514-z.
- [6] W. Zhang, D. Sun, L. Han, Y. Li, Optimised design of electrode morphology for novel dissimilar resistance spot welding of aluminium alloy and galvanised high strength steel, *Materials & Design*. 85 (2015) 461–470. doi:10.1016/j.matdes.2015.07.025.
- [7] Y. Zhang, J. Huang, Z. Cheng, Z. Ye, H. Chi, L. Peng, S. Chen, Study on MIG-TIG double-sided arc welding-brazing of aluminum and stainless steel, *Materials Letters*. 172 (2016) 146–148. doi:10.1016/j.matlet.2016.02.146.
- [8] S. Sarafan, P. Wanjara, H. Champliaud, D. Thibault, Characteristics of an autogenous single pass electron beam weld in thick gage CA6NM steel, *International Journal of Advanced Manufacturing Technology*. 78 (2015) 1523–1535. doi:10.1007/s00170-

014-6713-7.

- [9] R. S. Coelho, M. Corpas, J. A. Moreto, A. Jahn, J. Standfuß, A. Kaysser-Pyzalla, H. Pinto, Induction-assisted laser beam welding of a thermomechanically rolled HSLA S500MC steel: A microstructure and residual stress assessment, *Materials Science and Engineering A*. 578 (2013) 125–133. doi:10.1016/j.msea.2013.04.039.
- [10] J. Kim, Y. Kawamura, Electron beam welding of the dissimilar Zr-based bulk metallic glass and Ti metal, *Scripta Materialia*. 56 (2007) 709–712. doi:10.1016/j.scriptamat.2006.12.046.
- [11] S. K. Dinda, J. M. Warnett, M. A. Williams, G. G. Roy, P. Srirangam, 3D imaging and quantification of porosity in electron beam welded dissimilar steel to Fe-Al alloy joints by X-ray tomography, *Materials & Design*. 96 (2016) 224–231. doi:10.1016/j.matdes.2016.02.010.
- [12] N. Saresh, M. G. Pillai, J. Mathew, Investigations into the effects of electron beam welding on thick Ti-6Al-4V titanium alloy, *Journal of Materials Processing Technology*. 192–193 (2007) 83–88. doi:10.1016/j.jmatprotec.2007.04.048.
- [13] N. K. Babu, S. G. S. Raman, C. V. S. Murthy, G.M. Reddy, Influence of beam oscillation patterns on the structure and mechanical properties of Ti-6Al-4V electron beam weldments, *Science and Technology of Welding and Joining*. 10 (2005) 583–590. doi:10.1179/174329305X57473.
- [14] G. Sierra, P. Peyre, F. Deschaux-Beaume, D. Stuart, G. Fras, Steel to aluminium key-hole laser welding, *Materials Science and Engineering A*. 447 (2007) 197–208. doi:10.1016/j.msea.2006.10.106.
- [15] K. Bandyopadhyay, S. K. Panda, P. Saha, Investigations Into the Influence of Weld

- Zone on Formability of Fiber Laser-Welded Advanced High Strength Steel, *Journal of Materials Engineering and Performance*. 23 (2014) 1465–1479. doi:10.1007/s11665-014-0881-3.
- [16] J. Kar, S. K. Roy, G. G. Roy, Effect of beam oscillation on electron beam welding of copper with AISI-304 stainless steel, *Journal of Materials Processing Technology*. 233 (2016) 174–185. doi:10.1016/j.jmatprotec.2016.03.001.
- [17] I. Tomashchuk, P. Sallamand, N. Belyavina, M. Pilloz, Evolution of microstructures and mechanical properties during dissimilar electron beam welding of titanium alloy to stainless steel via copper interlayer, *Materials Science and Engineering A*. 585 (2013) 114–122. doi:10.1016/j.msea.2013.07.050.
- [18] P. Fu, Z. Mao, C. Zuo, Y. Wang, C. Wang, Microstructures and fatigue properties of electron beam welds with beam oscillation for heavy section TC4-DT alloy, *Chinese Journal of Aeronautics*. 27 (2014) 1015–1021. doi:10.1016/j.cja.2014.03.020.
- [19] S. Khaple, R. G. Baligidad, Effect of Melting Process on the Microstructure and Mechanical Properties of Fe–7 wt% Al Alloy, *Transactions of the Indian Institute of Metals*. 65 (2012) 57–61. doi:10.1007/s12666-011-0105-6.
- [20] S. Khaple, R. G. Baligidad, M. Sankar, V. V. Satya Prasad, Structure and properties of Fe–(3–7 wt.%) Al–0.5wt.%C alloys, *Materials Science and Engineering: A*. 527 (2010) 7452–7456. doi:10.1016/j.msea.2010.07.058.
- [21] J. Kar, S. Mahanty, S. K. Roy, G. G. Roy, Estimation of Average Spot Diameter and Bead Penetration Using Process Model During Electron Beam Welding of AISI 304 Stainless Steel, *Transactions of the Indian Institute of Metals*. (2015). doi:10.1007/s12666-015-0529-5.

- [22] Z. Zaczek, J. Cwiek, Prediction of HAZ Hardness in Welds of Quenched and Tempered HSLA Steels Carbon equivalent formulas are evaluated for accuracy in predicting the critical, *Welding Research Supplement*. (1993) 37-40.
- [23] S. F. Su, J. C. Huang, H. K. Lin, N. J. Ho, Electron-beam welding behavior in Mg-Al-based alloys, *Metallurgical and Materials Transactions A*. 33 (2002) 1461–1473. doi:10.1007/s11661-002-0069-6.

Accepted manuscript